AFCRL-72-0083
1 FEBRUARY 1972
PHYSICAL SCIENCES RESEARCH PAPERS, NO. 478

MICROWAVE PHYSICS LABORATORY PROJECT 5635

AIR FORCE CAMBRIDGE RESEARCH LABORATORIES

L. G. HANSCOM FIELD, BEDFORD, MASSACHUSETTS

Null Steering and Maximum Gain in Electronically Scanned Dipole Arrays

C.J. DRANE, JR.
J.F. Mc ILVENNA

AIR FORCE SYSTEMS COMMAND
United States Air Force

Unclassified

Security Classification

DOCUMENT CONTROL DATA - R&D

(Security classification of title, body of abstract and indexing annotation must be entered when the overall report is classified)

1 ORIGINATING ACTIVITY *(Corporate author)*
Air Force Cambridge Research Laboratories (LZ)
L. G. Hanscom Field
Bedford, Mass. 01730

2a. REPORT SECURITY CLASSIFICATION
Unclassified

2b. GROUP

3. REPORT TITLE

NULL STEERING AND MAXIMUM GAIN IN ELECTRONICALLY SCANNED DIPOLE ARRAYS

4. DESCRIPTIVE NOTES *(Type of report and inclusive dates)*
Station Report

5 AUTHOR(S) *(First name, middle initial, last name)*
C. J. Drane, Jr.
J. F. McIlvenna

6. REPORT DATE	7a. TOTAL NO OF PAGES	7b. NO. OF REFS
1 February 1972	38	24

8a. CONTRACT OR GRANT NO.		9a. ORIGINATOR'S REPORT NUMBER(S)
b. PROJECT, TASK, WORK UNIT NOS.	5635-06-01	AFCRL-72-0083
c. DOD ELEMENT	61102F	9b. OTHER REPORT NO(S) *(Any other numbers that may be assigned this report)* PSRP No. 478
d. DOD SUBELEMENT	681305	

10. DISTRIBUTION STATEMENT
Approved for public release; distribution unlimited

11. SUPPLEMENTARY NOTES	12. SPONSORING MILITARY ACTIVITY
TECH, OTHER	Air Force Cambridge Research Laboratories (LZR) L. G. Hanscom Field Bedford, Mass. 01730

13. ABSTRACT

A technique that simultaneously maximizes the gain of an antenna array and places a number of independent nulls in the radiation pattern has already been presented. The elements used were idealized point sources. In the present paper, the previous analysis is extended to cover arrays of thin wire elements in which interelement mutual coupling and scanning effects are included. Sample calculations and computed radiation patterns demonstrate that an appreciable amount of pattern and sidelobe control can be obtained with only a small sacrifice in gain.

DD FORM 1 NOV 65 1473

Unclassified

Security Classification

KEY WORDS	LINK A		LINK B		LINK C	
	ROLE	WT	ROLE	WT	ROLE	WT
Antenna gain Maximum directivity or gain Mutual coupling Antenna arrays Radiation pattern nulls Sidelobe control						

Abstract

A technique that simultaneously maximizes the gain of an antenna array and places a number of independent nulls in the radiation pattern has already been presented. The elements used were idealized point sources. In the present paper, the previous analysis is extended to cover arrays of thin wire elements in which interelement mutual coupling and scanning effects are included. Sample calculations and computed radiation patterns demonstrate that an appreciable amount of pattern and sidelobe control can be obtained with only a small sacrifice in gain.

Contents

Illustrations

Illustrations

Tables

Null Steering and Maximum Gain in Electronically Scanned Dipole Arrays

I. INTRODUCTION

In a recent paper (Drane and McIlvenna, 1970), the authors presented a technique for maximizing the gain of an antenna array, while at the same time placing one or a number of independent nulls and/or sidelobes in the far-field radiation pattern.* Some problem areas requiring such a technique include the elimination of jammer interference in radio-radar communications links, the reduction of ground reflections in sited antennas and the minimization of inter-antenna interference effects in multi-antenna environments. The sample computations in that earlier paper were restricted to arrays of idealized antenna elements, that is, isotropic radiators. It was pointed out there, however, that the "maximum gain - null placing" technique would be applicable even with arrays of elements (dipoles, for example) when interelement mutual coupling effects must, of necessity, be considered. Since that time, a particular method of design for arrays of wire elements (Strait and Hirasawa, 1968 and 1969a) which elegantly and practically accounts for mutual coupling effects has been combined with the aforementioned maximum gain - constraint technique. These design methods are discussed below together with some examples of practical interest.

(Received for publication 31 January 1972)

*Several papers on this and closely related subjects have appeared (Nemit, 1969; Sandrin and Glatt, 1970; Riegler and Compton, 1970; Pierce, 1970; Hessel and Sureau, 1971; Adams and Strait, 1970; Sanzgiri, et al, 1971).

2. DESIGN TECHNIQUES FOR ARRAYS OF WIRE ELEMENTS

The method summarized below is due to Strait and Harrington and has been reported in detail by Strait and Adams (1970), Chao and Strait (1971), Strait and Hirasawa (1970a), Hirasawa and Strait (1971a, 1971b), and Strait and Chao (1971). With it, the designer can determine such properties as the actual current distributions along the antenna elements, input and driving-point impedances and the radiation and scattered field patterns of arrays of parallel, staggered or even arbitrarily bent wires. The elements may be arbitrarily spaced, loaded or unloaded, lossy or lossless, center-fed or arbitrarily excited at points along their length, and they may be placed in any geometric arrangement. Even radiating elements with wire junctions such as crossed dipoles (Chao and Strait, 1971) can be handled. Most importantly, in every case mutual coupling effects are included. Detailed handbook-type reports with computer programs for a wide variety of array design problems are available by Strait and Hirasawa (1969b, 1970b), Chao and Strait (1970), and Mautz and Harrington (1971). Only the highlights of the technique are presented here; they lead to an expression for array gain with mutual coupling effects included.

Starting from the integral equation for a thin wire, one considers each antenna in the array to be subdivided into a number of segments, K (ten per wavelength has proven to be sufficient for far-field considerations), whose end-points are treated as the terminals of a multi-terminal pair network. The goal is to relate every terminal pair to every other terminal pair through a mutual impedance matrix. The two boundary conditions, that the tangential component of the electric field vector $\vec{E}$ must be zero on the surface of each conducting element and that the axial current must go to zero at the ends of the antenna, are included in the analysis.

Introducing column vectors I and V, each with K components that are respectively the segment currents and voltages,

$$I^T = \{ I_1, I_2, \ldots, I_K \}$$

and

$$V^T = \{ V_1, V_2, \ldots, V_K \},$$

where superscript T denotes the vector transpose operation, allows one to represent the array problem in terms of circuit theory format, that is,

$$V = \bar{\bar{Z}} I ,$$

where $\bar{Z}$, a (K × K) - element, symmetric complex matrix, is the mutual impedance matrix relating the voltage and current for any segment to the voltage and current for every other segment.

Methods for calculating the elements in $\bar{Z}$ for any array geometry are available (Strait and Hirasawa, 1969a). It has been shown that

$$Z_{k,n} = j\omega \mu_o \Delta\ell_n \Delta\ell_k \psi(n,k) + \frac{1}{j\omega\epsilon_o} [\psi(n^+,k^+) - \psi(n^-,k^-) - \psi(n^+,k^-) + \psi(n^-,k^-)],$$

where

$$\psi(n,k) = \frac{1}{4\pi\Delta\ell_n} \int_{\Delta\ell_n} \frac{\exp[-j\beta R_{kn}(z')]}{R_{kn}(z')} dz',$$

and $\Delta\ell_n$ is the length of the n^{th} segment, $R_{kn}(z')$ is the distance between the k^{th} and n^{th} segments and the superscripts + and - (in n^+ and n^-), denote the starting point and termination, respectively, of the n^{th} segment. The quantity ω is the operating angular frequency, β is the corresponding wave number, and ϵ_o and μ_o are the universal electric and magnetic constants. The only other approximations made in this analysis are that the current and charge are assumed to be constant over the length of each segment. Calculations and comparisons with other mutual coupling methods have shown that such assumptions are not overly restrictive (Strait and Hirasawa, 1969a). Resistive or reactive loading and element losses can be included simply by adding a load matrix $\bar{Z}_\ell$ to the $\bar{Z}$ matrix defined above (Hirasawa and Strait, 1971a).

Given an array geometry and a set of driving voltages, the segment currents, with all mutual effects included, are found quite simply from

$$I = \bar{Z}^{-1} V = \bar{Y} V,$$

where $\bar{Y}$ is the (K×K) admittance matrix. With these segment currents, all the parameters of interest to the array designer can be obtained. For example, the far-zone vector potential for z-directed current elements has only a z-component given by (Strait and Hirasawa, 1967a)

$$A_z(\theta,\phi) = \frac{\exp[-j\beta r]}{4\pi r} \sum_{n=1}^{K} \Delta\ell_n I_n \exp[j\beta(x_n \sin\theta\cos\phi + y_n \sin\theta \sin\phi + z_n \cos\theta)], \quad (1)$$

and the far-field amplitude pattern is

$$E(\theta, \phi) = -j\omega \mu_o A_z(\theta, \phi) \sin \theta.$$

In these expressions x_n, y_n and z_n are the Cartesian coordinates of the center of the n^{th} segment while r, θ and ϕ denote the polar coordinates of the far-field observation point.

A non-restrictive assumption that simplifies computations is to take all segment lengths to be equal. Defining an angle-dependent row vector $F(\theta, \phi)$ with K elements, that is,

$$F_n(\theta, \phi) = \exp [\, j\beta (x_n \sin \theta \cos \phi + y_n \sin \theta \sin \phi + z_n \cos \theta)\,], \quad 1 \le n \le K,$$

and replacing I by $\bar{Y}V$ leads to a matrix form for A_z, viz.,

$$A_z(\theta, \phi) = K_o [F(\theta, \phi) \bar{Y} V], \tag{2}$$

where

$$K_o = \frac{\exp [-j\beta r]}{4\pi r} \Delta \ell,$$

where Δ is the length common to all segments. One need only use the relations above and some standard definitions to develop an expression for antenna gain which includes the effects of mutual coupling (Strait and Hirasawa, 1969a).

Recall that power gain for an antenna is defined to be

$$G = 4\pi \frac{\text{power radiated in a particular direction}}{\text{total power input to array}} \tag{3}$$

The power radiated in a particular direction (θ_o, ϕ_o) is related to the far-field amplitude pattern by

$$P(\theta_o, \phi_o) = \frac{r^2 |E(\theta_o, \phi_o)|^2}{\eta_o},$$

where η_o is the impedance of free space. In terms of the matrix expressions above,

$$P(\theta_o, \phi_o) = \frac{1}{\eta_o}\left(\frac{\omega \mu_o \Delta \ell}{4\pi}\right)^2 \left[V^+ (F\bar{Y})^+ (F\bar{Y}) V\right] \sin^2 \theta,$$

where superscript + denotes the combined operations of complex conjugation and transposition. The denominator term in Eq. (3) can be handled by multi-port circuit theory techniques and is expressible in terms of the D driving-point voltages v_d and currents i_d as (Strait and Hirasawa, 1969a)

$$P_T = \sum_{d=1}^{D} \text{Real}\,(v_d\, i_d^*)\,.$$

Let I_D and V_D represent D-element vectors of the driving-point currents and voltages. In vector notation

$$P_T = \text{Real}\,(V_D\, I_D^*).$$

Let Y_D represent the (D × D) complex driving-point admittance matrix formed from Y by selecting only those elements that correspond to driving points (Strait and Hirasawa, 1969a). Because of the symmetry in Y_D,

$$P_T = V_D^+ (\text{Real}\,(Y_D))\, V_D$$

and Eq. (3) becomes

$$G = K_1 \frac{V^+ (F\bar{Y})^+ (F\bar{Y}) V}{V_D^+ (\text{Real}\,(\bar{Y}_D))\, V_D}\,, \tag{4}$$

where

$$K_1 = \sin^2 \theta \frac{(\omega \mu_o \Delta \ell)^2}{4\pi \eta_o}\,.$$

the numerator matrix $(F\bar{Y})^+(F\bar{Y})$ is a (K × K)-element matrix and the denominator matrix, Real $(\bar{Y}_D)$, is a (D × D)-element matrix.

In the authors' earlier paper (Drane and McIlvenna, 1970), the parameter optimized was directive gain in contrast to the power gain discussed above. The difference between the two gains lies only in the denominator term of Eq. (3). Directive gain utilizes the total power radiated, that is,

$$P_{Rad.} = \int_0^{2\pi} \int_0^{\pi} P(\theta, \phi) \sin\theta \, d\theta \, d\phi,$$

instead of the total power input to the array. When the radiating elements are lossless (the usual assumption), the two gain formulations are identical. In any case, however, directive gain is an upper bound for the power gain and is therefore often used as a comparative indicator of array performance. It can be calculated from the expressions for $P(\theta, \phi)$ given earlier. (See Appendix A for details.)

Note that, as yet, no assumptions about the number of feed points have been made. If for example, every segment is fed, then D = K, V_D = V, and both the numerator and denominator matrices in Eq. (4) are (K × K) element matrices. Usually, however, D < K, and, in fact, a very common array configuration has each antenna element center-fed, in which case, D = N. This center-fed assumption also provides some simplification in the numerator of Eq. (4). For perfectly conducting center-fed elements, the only non-zero entries in V are at the N driving points themselves. One may then delete all the elements in the numerator matrix $(F\bar{Y})^+ (F\bar{Y})$ which do not correspond to these feed points, denoting the resulting (N × N) deleted matrix as:

$$\bar{A} = (F\bar{Y})_D^+ (F\bar{Y})_D .$$

For example, in a two-element array with five segments per element (K = 10), the center-feed points correspond to segments 3 and 8, and one need retain only four of the original 100, that is (K × K) elements of the numerator matrix $(F\bar{Y})^+ (F\bar{Y})$, namely, those with corresponding pairs of indices (3, 3), (3, 8), (8, 3) and (8, 8). Thus, the center-fed assumption reduces the dimensions of the numerator and denominator matrices of Eq. (4) from (10 × 10), that is (K × K) to (2 × 2), that is, (N × N). The final form for the power gain of an N-element array of center-fed thin wires, with mutual effects accounted for, can then be written as

$$G = K_1 \frac{V_D^+ \bar{A} V_D}{V_D^+ \text{Real}(\bar{Y}_D) V_D} = K_1 \frac{V_D^+ \bar{A} V_D}{V_D^+ \bar{B} V_D} . \tag{5}$$

The numerator and denominator matrices in Eq. (5) are both Hermitian, $\bar{A}$ is a one-term dyad, $\bar{B}$ is positive definite, hence the maximum gain can be written down immediately as (Strait and Hirasawa, 1969a)

$$G^{max} = K_1 (F\bar{Y})_D^+ (\text{Real}(\bar{Y}_D))^{-1} (F\bar{Y})_D , \tag{6a}$$

and the voltages that produce it are given (to within a constant) by

$$V_D^{max} = (\text{Real } (\bar{Y}_D))^{-1}(F\bar{Y})_D \ . \qquad (6b)$$

Equations (5) and (6) serve as the starting points for the maximum gain-constraint technique.

3. THE CONSTRAINT METHOD

The technique for placing nulls in the far-field radiation pattern, while simultaneously maximizing gain, follows the steps outlined in the authors' earlier paper (Drane and McIlvenna, 1970). Placing nulls in the directions $\{ \theta_i, \phi_i \}$, $i = 1, 2, \ldots, M$, with $M \leq (N - 1)$, requires that $E(\theta, \phi)$ (or equivalently $A_z(\vartheta, \phi)$) be set to zero in the M desired directions. For the center-fed wires discussed earlier, we therefore generate a set of M linear, homogeneous constraint equations of the form

$$(F(\theta_i, \phi_i)\bar{Y})_D V_D = 0, \quad i = 1, 2, \ldots, M.$$

Each of these equations consists of the inner product of a D-element angle-dependent row vector

$$(F(\theta_i, \phi_i)\bar{Y})_D \ ,$$

henceforth referred to as the constraint vector, and the column vector of driving point voltages, V_D. These constraint equations are not directly solved for the driving voltages. Instead, their effect is introduced into the gain expression through a transformation as follows. Each one of the M constraint vectors is considered to be a particular row in a constraint matrix which thus has M rows and D columns. In the case of the center-fed wires being considered here, D = N. The rectangular $(M \times N)$ constraint matrix is made into a square $(N \times N)$ matrix, $\bar{C}$, by adding $(N - M)$ rows. These additional rows can be any collection of N-element independent vectors. For example, the simplest such collection could be $(N - M)$ rows or columns of the $(N \times N)$ identity matrix. The $(N \times N)$ matrix $\bar{C}$ is then orthogonalized, row by row, using any appropriate method (Guillemin, 1949); and the resulting $(N \times N)$ matrix, denoted as $\bar{P}$, contains all the constraint information and is now introduced into the gain expression via the transformation

$$V_D = \bar{P}^+ \mathbf{V} \quad \text{or} \quad \mathbf{V} = \bar{P} V_D.$$

Thus, from Eq. (5),

$$G = K_1 \frac{\mathbf{v}^+ \bar{A}_c \mathbf{v}}{\mathbf{v}^+ \bar{B}_c \mathbf{v}} ,$$

where

$$\bar{A}_c = \bar{P}\,\bar{A}\,\bar{P}^+ = \bar{P}\,(F\bar{Y})_D^+\,(F\bar{Y})_D\,\bar{P}^+ \equiv a_c a_c^+$$

and

$$\bar{B}_c = \bar{P}\,(\text{Real}\,(\bar{Y}_D))\,\bar{P}^+ .$$

Following the arguments outlined earlier, we discard the first M rows and columns in $\bar{A}_c$ and $\bar{B}_c$, leaving the abridged $(N - M) \times (N - M)$ element matrices $\bar{A}_a$ and $\bar{B}_a$, discard the first M entries in $\mathbf{v}$ (denoting the resultant abridged vector $\mathbf{v}_a$) and finally discard the first M entries in a_c (denoting the resultant vector a_a). Thus, the final quadratic form representation for array gain, with all the effects of mutual coupling and pattern constraints included is

$$\Gamma = K_1 \frac{\mathbf{v}_a^+ \bar{A}_a \mathbf{v}_a}{\mathbf{v}_a^+ \bar{B}_a \mathbf{v}_a} ;$$

the maximum constrained gain is

$$\Gamma^{max} = K_1\,(a_a^+ \bar{B}_a^{-1} a_a) \leq G^{max}$$

and the corresponding driving voltages are found from

$$V_\Gamma^{max} = \bar{P}_d^+ \bar{B}_a^{-1} a_a ,$$

where $\bar{P}_d$ is an $(N - M) \times N$-element matrix formed by deletion of the first M rows in the $(N \times N)$-element matrix $\bar{P}$.

These results verify the claim made in our earlier work that, even when mutual coupling is included, the form of the gain relation and the properties of the numerator and denominator matrices are unchanged. *

---

*An alternate constraint technique has been proposed by Adams and Strait (1970).

4. SOME EXAMPLES

One of the most common linear array configurations utilizes $\lambda/2$ elements uniformly spaced at $\lambda/2$ intervals. This geometry was used for the sample computations in this paper. There were 12 thin, straight, wire elements, oriented in the z-direction and spaced along the x-axis, with 5 segments per element. Strait and Hirasawa (1969b, 1970b), Chao and Strait (1970), and Mautz and Harrington (1971) provide the computer programs to consider other geometries and element types.

One of the problems ideally suited to the maximum gain - constraint technique is the elimination of interference, jamming or unwanted signals through control of the radiation pattern. Unconstrained maximum gain radiation patterns are characterized by the presence of a relatively high secondary peak, for example 13 dB below the main peak. These high secondary peaks make such arrays susceptible to jamming. One can use constraints in several different ways to reduce these high peaks; two possibilities are discussed in the examples below.

One corrective technique requires the use of a single constraint and replaces a secondary peak of the unconstrained maximum gain pattern with a null. A second approach is to use two closely spaced nulls to reduce the radiation level over an angular sector that includes the secondary peak. The first approach is useful when the angular location of the jamming source is exactly known. The second is more suitable when the location of the interfering source is not accurately known or when one desires to control a broader region in the pattern perhaps because the jamming source is of some significant angular extent. In both cases, the null or nulls should be maintained fixed in space even while the main beam is scanned all the way from broadside to endfire. Because of this wide range in scan angles, it is especially important to include mutual coupling effects. Figure 1 demonstrates the two techniques with the unconstrained broadside pattern of a 12-element, $\lambda/2$ - spaced array of thin-wire dipole elements, $\lambda/2$ long. All patterns are normalized to facilitate comparison. The secondary peak of the unconstrained maximum gain pattern at $\phi = 76^{\circ}$ is eliminated by the first technique or it can be reduced by the second technique. Note that the pattern structure is relatively unchanged, except in the vicinity of the enforced nulls. This demonstrates the localized pattern control available with the constraint method. The 3 dB beamwidths of all three patterns are almost identical, while the beamwidth between nulls of the constrained patterns increases only slightly. For the two-constraint case, the design criteria were as follows. The main beam should be scannable in the principal H-plane, but for every scan angle in that plane, the gain in the direction of the scan angle is maximum, while the radiation level is held at or below -30 dB over a 4° angular sector centered at $\phi = 76^{\circ}$. This minimal radiation level sector was created by

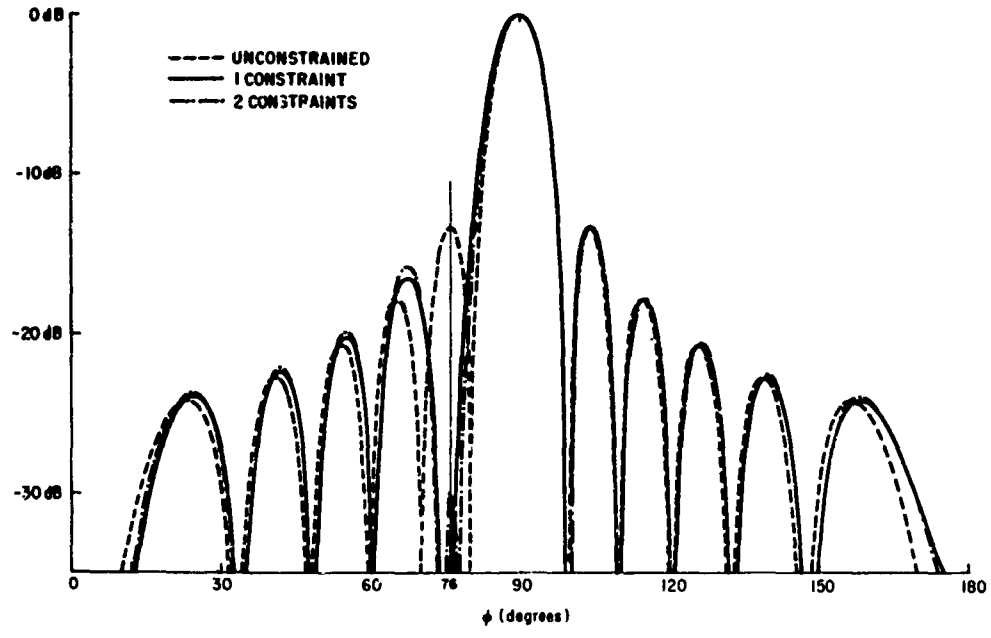

Figure 1. Broadside Beams

using two nulls, fixed in place (at $\phi = 74^{\circ}$ and $\phi = 78^{\circ}$) for all scan angles. The resultant patterns, for this two-constraint case plotted at 10° increments in the scan angle, are shown in Figure 2. Note in Figure 2(a) the well defined trough in the patterns, which is at least 4° wide at every scan angle and in which the highest radiation level is -30 dB for the broadside pattern and at least -35 dB for the other patterns. Figure 2(b) shows the gradual and expected broadening of the main beam and the buildup of the endfire lobes as scan angle increases, until at $\phi = 180^{\circ}$, the pattern is bifurcated. This splitting of the main beam into two equal lobes is characteristic of the $\lambda/2$ spacing chosen for this example.

Complete information for the unconstrained, one-constraint and two-constraint cases is presented in Table 1. Corresponding radiation pattern plots are shown in Figures 1, and 3 through 11.

Examining Table 1(a), we see that as mentioned earlier, constrained gains are less than or equal to the unconstrained gains. An interesting observation is the small amounts of gain that must be surrendered to obtain a desired degree of pattern control! In the one-constraint case, the largest loss occurs at broadside and represents only a 5 percent reduction in gain. In the two-constraint case, the largest loss is about 4 percent again at broadside, and in both the one- and two-constraint cases, the gain loss is less than about 2 percent over the range of other scan angles.

(a)

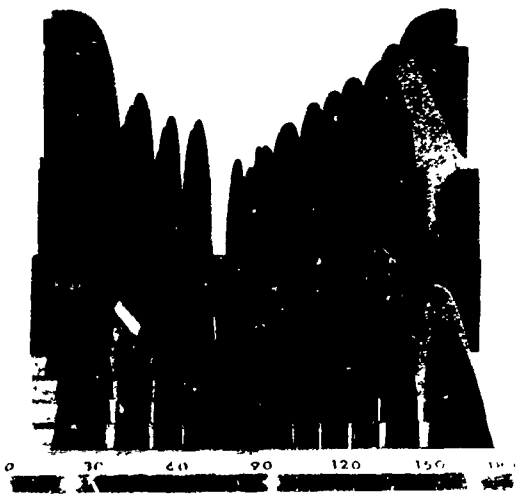

(b)

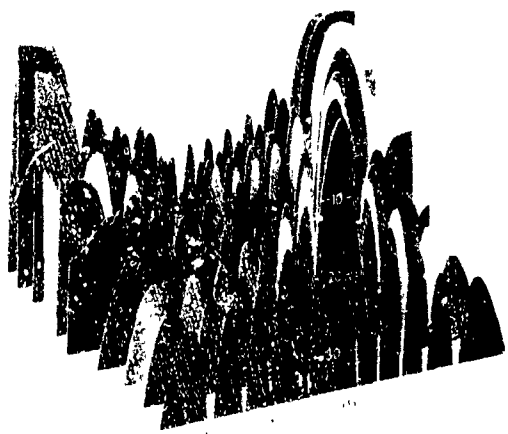

Figure 2. Resultant Patterns for Two-Constraint Case Plotted in 10^{o} Increments in Scan Angle

Table 1. Comparison of Unconstrained (U), One Constraint (C1) and Two Constraint (C2) Array Properties

Scan Angle	90° (broadside)			100°			110°			120°			130°		
	U	C(1)	C(2)	U	C(1)	C(2)	U	C(1)	C(2)	U	C(1)	C(2)	U	C(1)	C(2)
(a) Array Gain															
GAIN	25.92	24.64	24.97	25.29	24.81	24.93	23.59	23.33	23.39	21.26	21.10	21.09	18.80	18.74	18.54
(b) Voltage Distribution (Amplitude)															
Element Number 1	1.00	1.00	1.00	1.00	1.00	1.00	1.00	1.00	1.00	1.00	1.00	1.00	1.00	1.00	1.00
2	0.97	0.80	0.83	0.84	0.75	0.74	0.76	0.79	0.73	0.77	0.87	0.79	0.82	0.88	0.97
3	0.97	0.86	0.83	0.94	1.03	0.97	0.86	0.89	0.94	0.77	0.82	0.84	0.73	0.72	0.75
4	0.97	0.95	0.90	0.87	1.06	1.01	0.86	0.91	0.89	0.83	0.82	0.78	0.76	0.82	0.83
5	0.97	1.17	1.09	0.90	1.02	0.98	0.83	0.80	0.77	0.82	0.93	0.90	0.82	0.81	0.87
6	0.97	1.25	1.17	0.90	0.87	0.85	0.84	0.84	0.90	0.80	0.82	0.80	0.82	0.87	0.89
7	0.97	1.29	1.21	0.89	0.84	0.92	0.84	0.96	0.92	0.81	0.85	0.83	0.78	0.80	0.92
8	0.97	1.15	1.08	0.89	1.01	0.97	0.86	0.82	0.80	0.80	0.90	0.86	0.75	0.77	0.83
9	0.97	1.03	0.96	0.92	1.11	1.06	0.83	0.87	0.85	0.78	0.77	0.74	0.79	0.84	0.83
10	0.97	0.82	0.80	0.85	0.93	0.88	0.82	0.97	0.92	0.83	0.92	0.92	0.86	0.85	0.94
11	0.97	0.84	0.84	0.96	0.92	0.89	0.92	0.94	0.89	0.88	0.94	0.87	0.85	0.90	0.90
12	1.00	0.96	0.97	0.85	0.82	0.84	0.75	0.72	0.73	0.68	0.65	0.68	0.64	0.62	0.65
(c) Voltage Distribution (Phase)															
Element Number 1	0°	0°	0°	0°	0°	0°	0°	0°	0°	0°	0°	0°	0°	0°	0°
2	-18°	-13°	-16°	-15°	-5°	-9°	-7°	3°	2°	2°	6°	12°	6°	5°	17°
3	-10°	8°	3°	-11°	2°	1°	-12°	-8°	-7°	-6°	-9°	-5°	3°	2°	2°
4	-15°	10°	6°	-10°	-2°	-3°	-8°	-11°	-10°	-6°	-2°	-1°	-3°	-2°	7°
5	-12°	10°	7°	-11°	-13°	-12°	-9°	-3°	-5°	-3°	-1°	3°	-2°	-5°	-1°
6	-13°	3°	0°	-10°	-9°	-10°	-11°	-3°	-3°	-4°	-6°	-3°	1°	2°	8°
7	-13°	-5°	-7°	-11°	2°	1°	-11°	-13°	1°	-4°	2°	5°	2°	-2°	4°
8	-12°	-11°	-13°	-10°	2°	1°	-11°	-9°	-8°	-3°	-4°	-2°	-2°	0°	6°
9	-15°	-16°	-17°	-9°	-3°	-4°	-10°	-1°	-1°	-4°	-5°	0°	-5°	8°	-4°
10	-10°	-6°	-6°	-9°	-11°	-11°	-15°	-12°	-13°	-7°	-2°	0°	-3°	-2°	8°
11	-18°	-4°	-5°	-12°	-9°	-8°	-12°	-13°	-11°	-1°	-3°	0°	4°	2°	3°
12	0°	25°	21°	5°	20°	18°	0°	9°	10°	8°	12°	20°	9°	3°	26°
(d) Linear Progressive Phase Shift Required to Scan Beam															
	0°			31°			62°			90°			116°		

Table 1 (Contd). Comparison of Unconstrained (U), One Constraint (C1) and Two Constraint (C2) Array Properties

(a) Array Gain															
Scan Angle	140°			150°			160°			170°			180°		
	U	C1	C2	U	C1	C2	U	C1	C2	U	C1	C2	U	C1	C2
GAIN	16.59	16.59	16.26	14.85	14.76	14.76	13.71	13.71	13.42	13.34	13.27	13.22	13.32	13.22	13.20
(b) Voltage Distribution (Amplitude)															
Element Number 1	1.00	1.00	1.00	1.00	1.00	1.00	1.00	1.00	1.00	1.00	1.00	1.00	1.00	1.00	1.00
2	0.92	0.92	1.15	1.01	1.09	1.06	1.05	1.05	1.17	1.09	1.07	1.16	1.10	1.09	1.14
3	0.82	0.81	0.85	1.00	1.02	1.03	1.07	1.07	1.19	1.12	1.16	1.21	1.15	1.20	1.22
4	0.73	0.73	0.89	0.99	1.04	1.01	1.07	1.07	1.12	1.14	1.12	1.16	1.18	1.16	1.18
5	0.69	0.68	0.74	0.97	1.02	1.02	1.06	1.06	1.19	1.15	1.15	1.23	1.19	1.21	1.24
6	0.71	0.71	0.82	0.95	0.97	0.96	1.04	1.04	1.13	1.14	1.17	1.22	1.20	1.24	1.26
7	0.77	0.77	0.88	0.93	1.00	0.99	1.02	1.01	1.10	1.14	1.11	1.17	1.20	1.18	1.20
8	0.84	0.84	0.92	0.90	0.88	0.90	0.98	0.99	1.07	1.12	1.15	1.20	1.19	1.24	1.26
9	0.88	0.88	1.05	0.87	0.94	0.93	0.94	0.93	1.05	1.10	1.09	1.17	1.18	1.18	1.22
10	0.87	0.87	0.91	0.82	0.81	0.80	0.88	0.88	0.89	1.06	1.06	1.07	1.15	1.15	1.15
11	0.79	0.78	0.96	0.74	0.80	0 80	0.80	0.80	0.94	1.00	1.04	1.10	1.10	1.15	1.18
12	0.58	0.58	0.54	0.58	0.58	0.55	0.65	0.65	0.63	0.89	0.86	0.91	1.00	0.97	1.00
(c) Voltage Distribution (Phase)															
Element Number 1	0°	0°	0°	0°	0°	0°	0°	0°	0°	0°	0°	0°	0°	0°	0°
2	9°	12°	9°	9°	8°	5°	8°	8°	1°	5°	3°	2°	4°	1°	1°
3	15°	15°	19°	14°	16°	14°	12°	12°	13°	8°	6°	3°	5°	4°	5°
4	14°	14°	12°	16°	14°	23°	16°	16°	13°	10°	9°	9°	6°	6°	6°
5	8°	8°	10°	18°	21°	19°	19°	19°	17°	11°	8°	9°	7°	3°	4°
6	3°	3°	3°	19°	18°	16°	22°	22°	20°	12°	12°	13°	7°	6°	7°
7	0°	0°	0°	21°	23°	21°	44°	44°	42°	13°	11°	12°	7°	5°	6°
8	2°	2°	3°	22°	22°	20°	26°	26°	23°	14°	12°	12°	7°	4°	5°
9	6°	6°	5°	23°	24°	22°	28°	28°	28°	23°	14°	16°	8°	6°	7°
10	12°	12°	16°	24°	26°	23°	30°	29°	27°	15°	12°	13°	6°	2°	4°
11	19°	17°	13°	24°	23°	22°	31°	31°	27°	14°	13°	12°	4°	3°	3°
12	19°	19°	29°	26°	25°	20°	30°	29°	35°	12°	10°	15°	0°	1°	2°
(d) Linear Progressive Phase Shift Required to Scan Beam															
	138°			156°			169°			177°			180°		

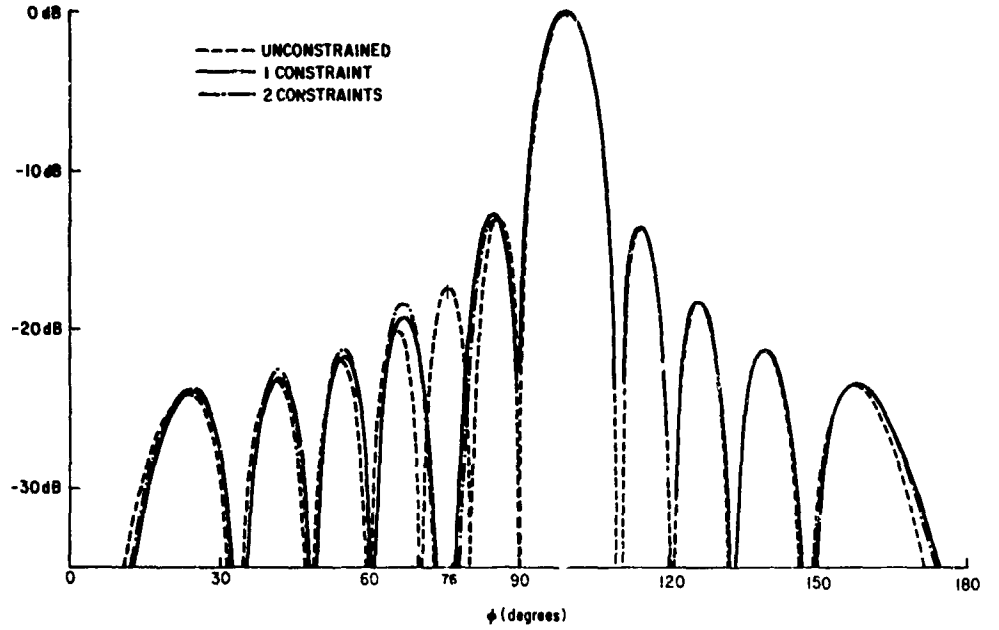

Figure 3. Beam Scanned to 100°

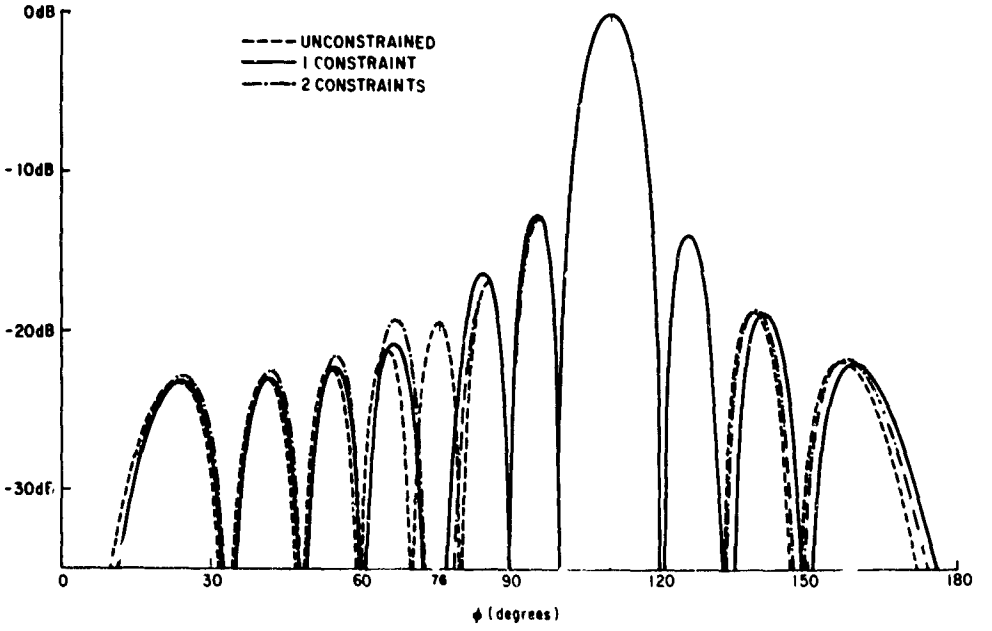

Figure 4. Beam Scanned to 110°

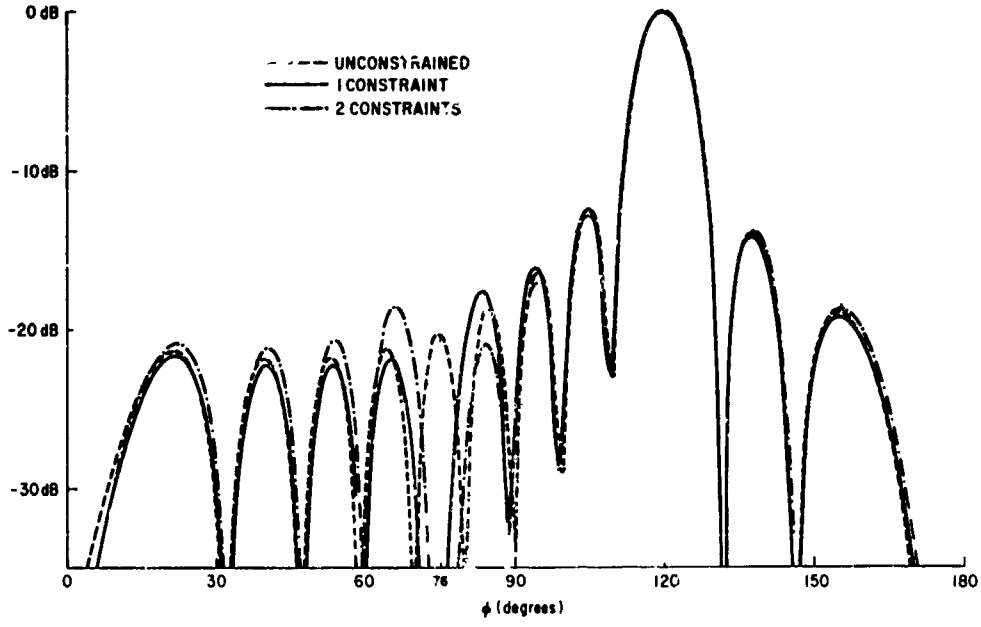

Figure 5. Beam Scanned to 120°

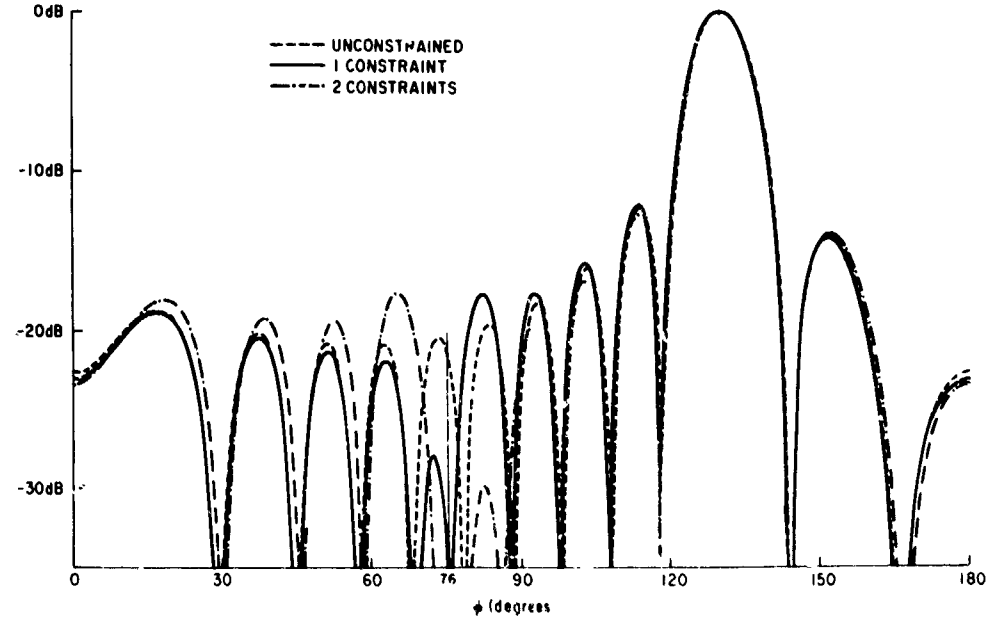

Figure 6. Beam Scanned to 130°

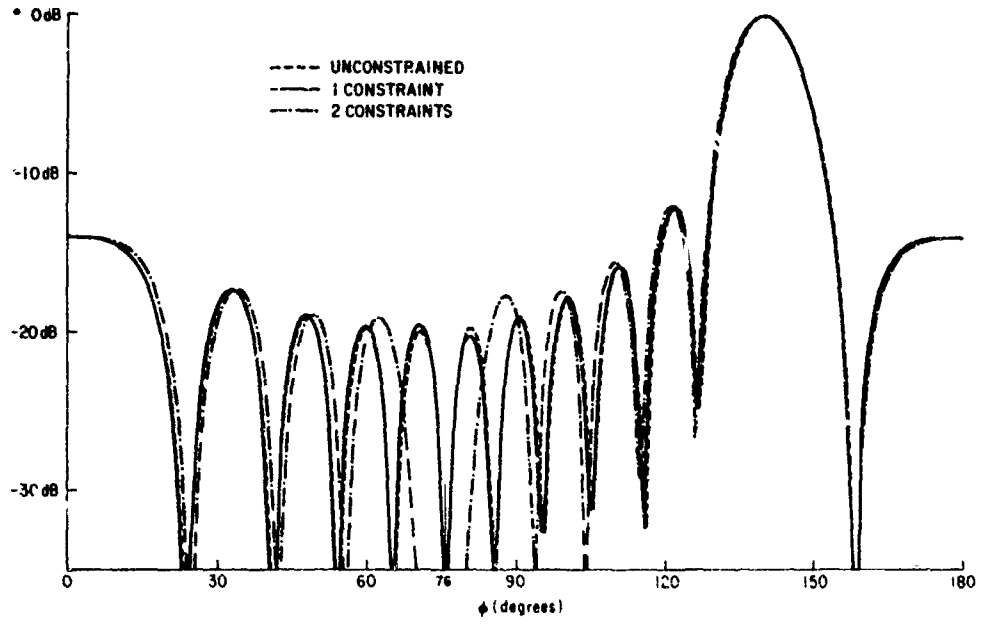

Figure 7. Beam Scanned to 140°

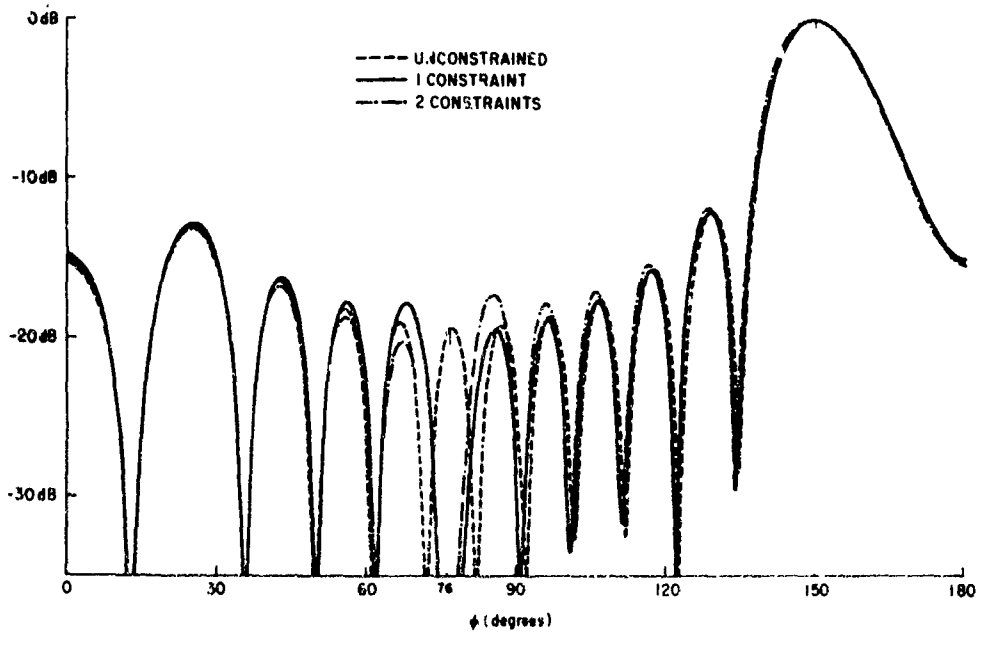

Figure 8. Beam Scanned to 150°

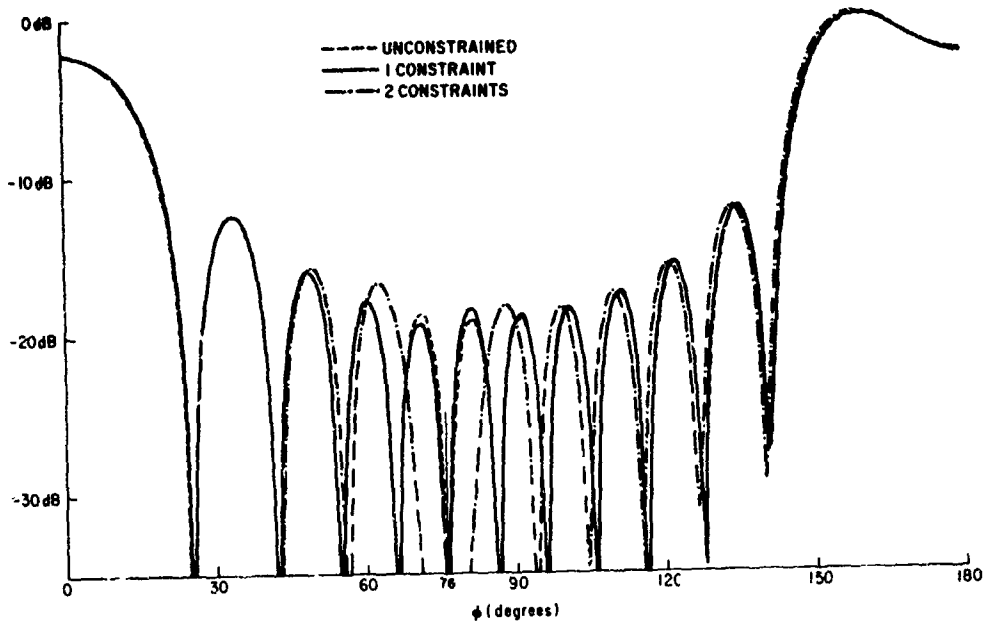

Figure 9. Beam Scanned to 160°

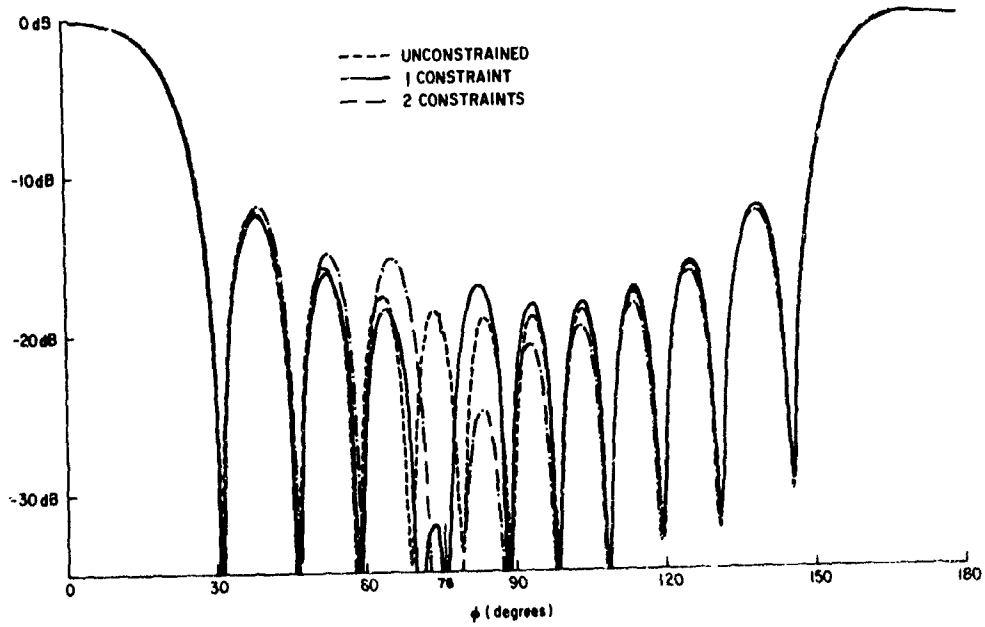

Figure 10. Beam Scanned to 170°

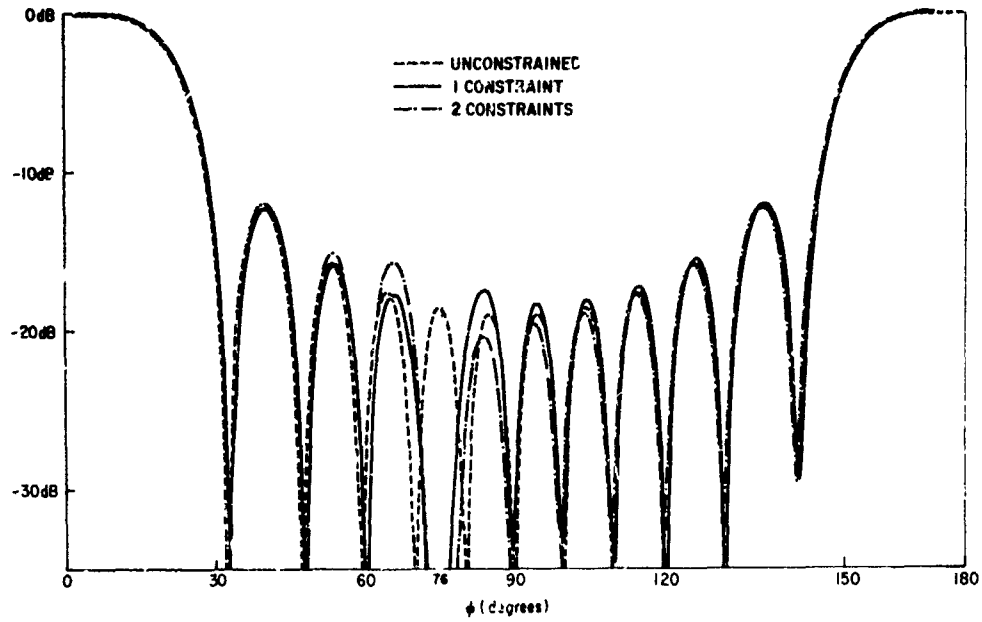

Figure 11. Beam Scanned to 180°

We also see that for some scan angles, that is 90° to 110°, the gain in the two-constraint case is higher than in the one-constraint case. This is simply explained. Controlling the value of the secondary peak to -30 dB as done in the two constraint case represents less of a constraint on the pattern behavior at these angles than does forcing that same peak value to be zero, as is done in the one-constraint case. It thus does not necessarily follow that the gain decrease is directly proportional to the number of null constraints used. Only when the constraints are used to perform the same function on the pattern will the gain decrease be proportional to the number of constraints. For example, replacing two peaks with nulls causes more gain loss than replacing one peak with a null, and replacing three peaks with nulls causes even more of a gain loss, and so on. This type of dependence, linking gain loss to number of enforced nulls, is the only one that can be identified.

Generally speaking, the decrease in gain value caused by pattern constraints is proportional to the value of the unconstrained pattern in the immediate vicinity of the enforced nulls. For example, as seen above and in Figure 1, at broadside the constraint region includes a significant secondary peak of the unconstrained pattern and the gain loss is largest; when the unconstrained pattern value in the constraint region becomes smaller, the gain loss is less. For example, at 140°

and 160°, the unconstrained pattern already has a null at $\phi = 76°$, implying that the one constraint case is in actuality no constraint at all. There is therefore no loss in gain, the amplitude and phase distributions are almost identical and the unconstrained and one constraint patterns are quite similar (see Figures 7 and 9).

An examination of the voltage amplitude distributions in Table 1(b), (each distribution is normalized to the voltage for its first element) reveals that these maximum gain voltages, constrained and unconstrained, are all non-uniform and most are non-symmetric about the center of the array. The only two symmetric distributions (the broadside and endfire unconstrained cases) correspond to the only two radiation patterns that are symmetric about the broadside angle $\phi = 90°$. Note that in some cases the voltage required for element 12 differs significantly from the voltages for all other elements. It also appears that for certain scan angles, for example 150°, the difference between the unconstrained and constrained amplitude distributions is small. As was true for the earlier comparison of the corresponding gain values, the explanation here is that at some scan angles the unconstrained pattern values are either very small in the constraint region, or the direction for one of the unconstrained nulls is nearly the same as that of one of the constraints. The constraint condition therefore requires only a slight perturbation of the unconstrained voltage distribution in these cases. Finally, note that in no case is the dynamic range of the driving-point voltages excessive. Compared to the ten-to-one variation usually taken as the practical limit of realizability, the range for both constrained and unconstrained optimum distributions is less than about two-to-one, and the distributions should offer no construction problems. The phase distributions for these maximum gain arrays can be considered to consist of the superposition of several components. The first is the uniform progressive phase taper that steers the beam to the desired scan angle and is common to all electronically scanned arrays, constrained or unconstrained. The second taper is that required to maximize the gain. And, in the constrained cases, an additional taper is required to place the pattern nulls as prescribed. Table 1(c) shows the unconstrained and constrained normalized phase distributions, after the beam steering phase distribution (shown for reference in Table 1(d)) has been removed. As in the case of the voltage distributions, note here also that the phase distributions are non-uniform and that most are non-symmetric. Finally, keep in mind that the examples discussed in this paper, and indeed in most expected applications, even though the designer directly controls the sidelobe level in only some local region of the radiation pattern, additional control, as a direct result of the application of these constraints will not become necessary over the remainder of the sidelobe region (Sanzgiri and Butler, 1971). This is due to the general phenomenon that reasonably low sidelobes are an intrinsic concomitant to maximization of gain.

5. CONCLUSIONS

We conclude that even with mutual coupling accounted for, the maximum gain - constraint technique provides realistic and practical solutions to array design problems requiring localized pattern control. The technique is applicable to practically all arrays of wire elements, regardless of their geometric arrangement and their electrical loading characteristics. The required relations and equations can be cast in matrix form and are ideally suited to computer manipulation, making them useful in adaptive or real-time situations requiring rapid pattern reconfiguration.

Acknowledgments

The authors wish to express their appreciation to Mrs. Evelyn Jones of the Experimental Fabrication Section (SURSF) at AFCRL for all her help in providing the radiation pattern models used in Figure 2.

References

Adams, A. T. and Strait, B. J. (1970) Modern analysis methods for EMC, IEEE EMC Symposium Record, pp 383-393.

Chao, H. H. and Strait, B. J. (1970) Computer Programs for Radiation and Scattering by Arbitrary Configurations of Bent Wires, Scientific Report No. 7 on Contract F19628-68-C-0180, Report No. AFCRL-70-0374.

Chao, H. H. and Strait, B. J. (1971) Radiation and scattering by configurations of bent wires with junctions, IEEE Trans. AP AP-19 (No. 5):71.

Drane, C. J., and McIlvenna, J. F. (1970) Gain maximization and controlled null placement simultaneously achieved in aerial array patterns, AFCRL Research Report 69-0257, June 1969. Subsequently published in The Radio and Electronic Engineer, 39 (No. 1):49-57.

Guillemin, E. A. (1949) The Mathematics of Circuit Analysis, The Technology Press, Cambridge, Mass.

Hessel, A. and Sureau, J. C. (1971) On the realized gain of arrays, IEEE Trans. AP AP-19 (No. 1):122-124.

Hirasawa, K. and Strait, B. J. (1971a) Analysis and Design of Arrays of Loaded Thin Wires by Matrix Methods, Scientific Report No. 12 on Contract F19628-68-C-0180, Report No. AFCRL-71-0296.

Hirasawa, K. and Strait, B. J. (1971b) On a method for array design by matrix inversion, IEEE Trans. G-AP AP-19 (No. 3):446-447.

Lo, Y. T., Lee, S. W., and Lee, Q. H. (1966) Optimization of directivity and signal-to-noise ratio of an arbitrary antenna array, Proc. IEEE 54:1033-1045.

Magnus and Oberhettinger (1949) Functions of Mathematical Physics, New York, pp 30.

Mautz, J. R. and Harrington, R. F. (1971) Computer Programs for Characteristic Modes of Wire Objects, Scientific Report No. 11 on Contract F19628-68-C-0180, Report No. AFCRL-71-0174.

Nemit, J. T. (1969) Reduction of Phased Array Sidelobes Toward the Ground by Phase Control, Report No. 1609P, Wheeler Labs. Inc., Smithtown, N.Y.

Pierce, J. N. (1970) Receiving Array Coefficients That Minimize Interference and Noise, AFCRL-71-0079.

Riegler, R. L. and Compton, R. T. (1970) An Adaptive Array for Interference Rejection, Report No. 2552-4, Ohio State University.

Sandrin, W. A. and Glatt, C. R. (1970) Computer aided design of optimal linear phased arrays, The Microwave Journal, pp 57-64.

Sanzgiri, S. M. and Butler, J. K. (1971) Constrained optimization of the performance indices of arbitrary array antennas, IEEE Trans. AP AP-19:493-498.

Strait, B. J. and Adams, A. T. (1970) Analysis and design of wire antennas with applications to EMC, IEEE Trans. EMC EMC-12:45-54.

Strait, B. J. and Chao, H. H. (1971) Radiation and scattering by wire structures, IEEE Intl. Convention Digest, N.Y.

Strait, B. J. and Hirasawa, K. (1968) Array design by matrix methods, IEEE Trans. AP. AP-17:237-239, Mar. 1969, or Report AFCRL-68-0542, Oct. 1968, AD 678-089.

Strait, B. J., and Hirasawa, K. (1969a) Applications of Matrix Methods to Array Antenna Problems, Scientific Report No. 2 on Contract F19628-6 -C-0180, Report AFCRL-69-0158, AD 687-481.

Strait, B. J. and Hirasawa, K. (1969b) Computer Programs for Radiation, Reception and Scattering by Loaded Straight Wires, Scientific Report No. 3 on Contract F19628-68-C-0180, Report No. AFCRL-69-0440.

Strait, B. J. and Hirasawa, K. (1970a) On long wire antennas with multiple excitations and loadings, IEEE Trans. AP AP-18:699-700.

Strait, B. J. and Hirasawa, K. (1970b) Computer Programs for Analysis and Design of Linear Arrays of Loaded Wire Antennas, Scientific Report No. 5 on Contract F19628-68-C-0180, Report No. AFCRL-70-0108.

Tai, C. T. (1964) The optimum directivity of uniformly spaced broadside arrays of dipoles, IEEE Transactions G-AP AP-12:447-454.

Appendix A

Derivation of a Relation for the Directive Gain of an Array of Electrically Thin, Straight Wires With Mutual Coupling Effects Included

It was pointed out in the text that the expressions for directive gain and power gain differ only in the form of the denominator term. Power gain used the total power input to the array while directive gain uses the total power radiated. These are the same when the system is lossless. In all other cases, directive gain serves as an upper bound on the power gain and is often used as a performance criterion in array design. This latter expression is given in general by

$$P_{Rad.} = \frac{1}{4\pi} \int_0^{2\pi} \int_0^{\pi} P(\theta,\phi) \sin\theta \, d\phi \, d\theta,$$

where $P(\theta,\phi)$, the power pattern of the array, can be expressed as

$$P(\theta,\phi) = \frac{r^2}{\eta_o} \left| E(\theta,\phi) \right|^2 = K \left| A_z(\theta,\phi) \right|^2 \sin^2\theta$$

and $K = (r\omega\mu_o)^2/\eta_o$. This integral has been evaluated by Tai (1964) and Lo et al (1966) for isotropic sources and short dipoles. For the case of electrically thin, z-directed wires, spaced along the x-axis, $A_z(\theta,\phi)$ is given by

$$A_z(\theta,\phi) = \frac{\exp[-j\beta r]}{4\pi r} \sum_{n=1}^{K} \Delta\ell_n I_n \exp[j\beta(x_n \sin\theta\cos\phi + z_n \cos\theta)].$$

Taking all segments to be of equal length leads to

$$P_{Rad.} = \frac{1}{\eta_o}\left(\frac{\omega\mu_o \Delta\ell}{4\pi}\right)^2 \sum_{n=1}^{K} \sum_{m=1}^{K} I_n b_{nm} I_m^* , \tag{A1}$$

where

$$b_{nm} = \frac{1}{4\pi} \int_0^{2\pi} \int_0^{\pi} \exp[j(D_{nm} \sin\theta\cos\phi + E_{nm}\cos\theta)] \sin^3\theta \, d\phi \, d\theta,$$

and

$$D_{nm} = \beta(x_n - x_m), \quad E_{nm} = \beta(z_n - z_m).$$

The b_{nm} terms depend only on the array geometry and in no way are modified by the inclusion or exclusion of mutual coupling effects. But, the I_n quantities do indeed depend for their values on mutual coupling considerations. In matrix notation, Eq. (A1) becomes

$$P_{Rad} = \frac{1}{\eta_o}\left(\frac{\omega\mu_o\Delta\ell}{4\pi}\right)^2 I^+ \bar{\beta}\, I = \frac{1}{\eta_o}\left(\frac{\omega\mu_o\Delta\ell}{4\pi}\right)^2 V^+ (\bar{Y}^+ \bar{\beta}\, \bar{Y})\, V. \tag{A2}$$

The integration on ϕ in the expression for b_{nm} is readily performed (Jahnke and Emde, Pg. 149), that is,

$$\int_0^{2\pi} \exp[j D_{nm} \sin\theta\cos\phi]\, d\phi = 2\pi J_o(D_{nm} \sin\theta).$$

Thus

$$b_{nm} = \frac{1}{2} \int_0^{\pi} J_o(D_{nm} \sin\theta) \exp[j E_{nm} \cos\theta] \sin^3\theta \, d\theta.$$

This integral may be evaluated as follows. Note that about $\theta = \pi/2$, $\sin^3\theta$ and $J_o(D_{nm} \sin\theta)$ are even functions of θ, while $\sin(E_{nm}\cos\theta)$ is odd. Hence, we can discard the imaginary part of b_{nm} and, using the evenness of the real part, we have

$$b_{nm} = \int_0^{\pi/2} J_o (D_{nm} \sin\theta) \cos (E_{nm} \cos\theta) \sin^3\theta \, d\theta. \tag{A3}$$

Since

$$\sin^3\theta = \sin\theta (1 - \cos^2\theta)$$

and

$$\cos (E_{nm} \cos\theta) = \sum_{i=o}^{\infty} \frac{(-1)^i (E_{nm} \cos\theta)^{2i}}{(2i)!},$$

we can write

$$b_{nm} = \sum_{i=o}^{\infty} \frac{(-1)^i (E_{nm})^{2i}}{(2i)!} \left[\int_0^{\pi/2} J_o (D_{nm} \sin\theta) (\cos\theta)^{2i} \sin\theta \, d\theta \right.$$

$$\left. - \int_0^{\pi/2} J_o (D_{nm} \sin\theta) (\cos\theta)^{2i+2} \sin\theta \, d\theta \right].$$

Integrals of this same form were treated by Lo et al (1966) using the relation (Magnus and Oberhettinger, 1949)

$$\int_0^{\pi/2} J_\mu (z \sin\theta) \sin^{\mu+1}\theta \cos^{2v+1}\theta \, d\theta = \frac{2^v \Gamma(v+1) J_{v+\mu+1}(z)}{z^{v+1}}, \quad \mathrm{Re}\mu, \mathrm{Re}v > -1.$$

Thus

$$b_{nm} = \sum_{i=o}^{\infty} \frac{(-1)^i (E_{nm})^{2i}}{(2i)!} \left[\frac{2^{i-1/2} \Gamma(i+1/2) J_{i+1/2}(D_{nm})}{(D_{nm})^{i+1/2}} \right.$$

$$\left. - \frac{2^{i+1/2} \Gamma(i+3/2) J_{i+3/2}(D_{nm})}{(D_{nm})^{i+3/2}} \right].$$

Recall that

$$\Gamma(i+3/2) = (i+1/2) \Gamma(i+1/2),$$

$$(2i)! = \Gamma(1+2i) = \Gamma[2(i+1/2)],$$

and that

$$\Gamma(2z) = \frac{2^{2z-1}\,\Gamma(z)\,\Gamma(z+1/2)}{(\pi)^{1/2}} .$$

Thus

$$b_{nm} = \sqrt{\frac{\pi}{2}} \sum_{i=0}^{\infty} \frac{(-1)^i (E_{nm})^{2i}}{2^i\, i!} \left[\frac{J_{i+1/2}(D_{nm})}{(D_{nm})^{i+1/2}} - \frac{2(i+1/2)\, J_{i+3/2}(D_{nm})}{(D_{nm})^{i+3/2}} \right] , \quad m \neq n \tag{A4}$$

and $b_{nn} = 2/3$.

Note that

$$D_{mn} = -D_{nm}$$

$$E_{mn} = -E_{nm}$$

$$J_{i+1/2}(D_{mn}) = (-1)^{i+1/2} J_{i+1/2}(D_{nm})$$

$$J_{i+3/2}(D_{mn}) = (-1)^{i+3/2} J_{i+3/2}(D_{nm}),$$

hence $b_{mn} = b_{nm}$ and $\overline{\beta}$ is a real, symmetric matrix. Both m and n range from 1 to K, where K is the total number of segments in an N-element array. K can be rather large; for example, in the arrays considered in this paper, 12-elements with 5 segments per element, K = 60. Fortunately, however, one needs to calculate all 1800 of the b_{mn} elements only for the most general array geometries, that is, wires of arbitrary length and shape, arbitrarily spaced and located. In most arrays of practical interest, significantly less calculation is required. For equally spaced arrays of N straight wires, with S segments per wire, only NS or K of the 1800 elements in $\overline{\beta}$ are distinct. To see this, refer to Figure A1 taking N = 12 elements and S = 5 segments per element. Each of the twelve antenna elements gives rise to 25 b_{mn} terms. These (5 × 5) - element square submatrices are situated symmetrically about the main diagonal in $\overline{\beta}$; hence the submatrix diagonal terms are known to be 2/3. Because of the symmetry in $\overline{\beta}$, only 10 of the remaining 20 terms in any main diagonal submatrix can be distinct. One such submatrix, that associated with the first element, is shown below.

$$\bar{\beta}_1 = \begin{vmatrix} 2/3 & b_{12} & b_{13} & b_{14} & b_{15} \\ b_{12} & 2/3 & b_{23} & b_{24} & b_{25} \\ b_{13} & b_{23} & 2/3 & b_{34} & b_{35} \\ b_{14} & b_{24} & b_{34} & 2/3 & b_{45} \\ b_{15} & b_{25} & b_{35} & b_{45} & 2/3 \end{vmatrix} .$$

Each one of the 10 required b_{nm} terms depends on both a D_{nm} and an E_{nm} term. If the wire is straight and parallel to the z-axis, all 5 segments on that wire have the same x-coordinate and $D_{nm} = 0$ for all 10 of the desired elements in $\bar{\beta}_1$. If, in addition, all segments are chosen to be equal, then

$$E_{12} = E_{23} = E_{34} = E_{45}$$

$$E_{13} = E_{24} = E_{35}$$

$$E_{14} = E_{25} .$$

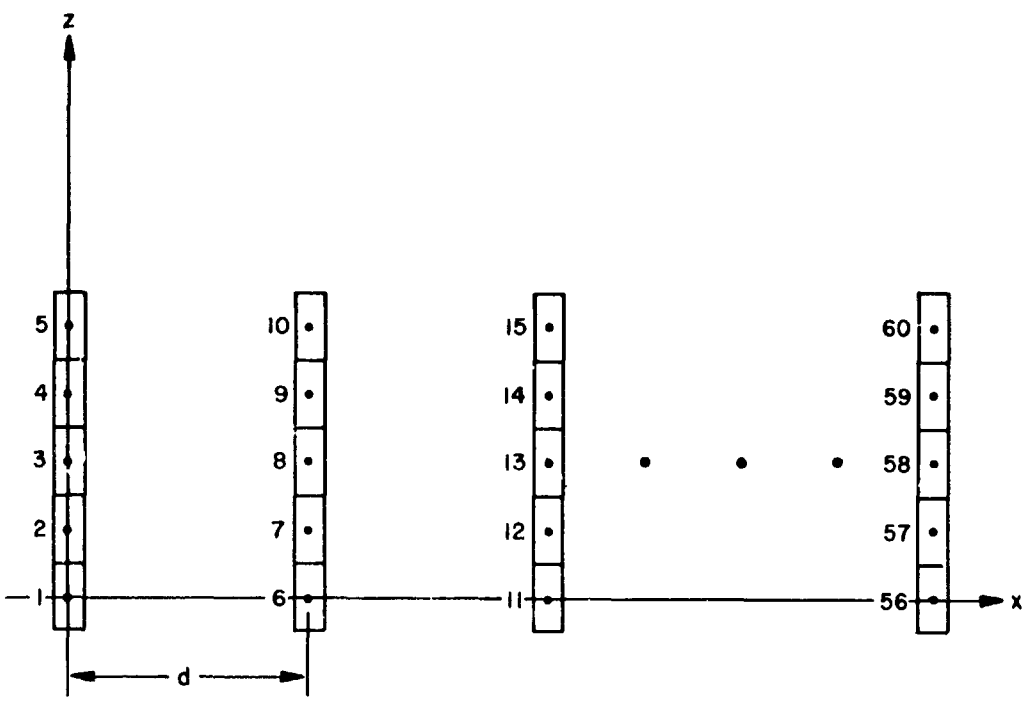

Figure A1. 12-Element Array, 5-Segments per Element

Hence,

$$b_{12} = b_{23} = b_{34} = b_{45}$$

$$b_{13} = b_{24} = b_{35}$$

$$b_{14} = b_{25} ,$$

and only 5 elements are needed to completely specify $\overline{\beta}_1$. Its final form is

$$\overline{\beta}_1 = \begin{vmatrix} 2/3 & b_{12} & b_{13} & b_{14} & b_{15} \\ b_{12} & 2/3 & b_{12} & b_{13} & b_{14} \\ b_{13} & b_{12} & 2/3 & b_{12} & b_{13} \\ b_{14} & b_{13} & b_{12} & 2/3 & b_{12} \\ b_{15} & b_{14} & b_{13} & b_{12} & 2/3 \end{vmatrix} .$$

If all the elements in the array are identical, then all of the 12 main diagonal submatrices are identical to $\overline{\beta}_1$ and 300 elements in $\overline{\beta}$ are determined with only four b_{nm} calculations.

The off-diagonal submatrices in $\overline{\beta}$ depend on the array spacing. Each pair of elements in the array gives rise to a 25 term submatrix and for a K-element array, there are 66 of these. In any one of these submatrices, if the two antenna elements in question are straight and parallel, all D_{nm} terms are the same and have the value βd where d is the interelement separation. As in $\overline{\beta}_1$ there are only 5 distinct E_{nm} values, hence once again only 5 calculations are needed to determine all 25 terms in any of the submatrices. The submatrix, $\overline{\beta}_2$, representative of the first two array elements, is shown below. It has the same type of symmetry and row regularity as $\overline{\beta}_1$, sometimes called a Toeplitz property.

$$\overline{\beta}_2 = \begin{vmatrix} b_{16} & b_{17} & b_{18} & b_{19} & b_{1,10} \\ b_{17} & b_{16} & b_{17} & b_{18} & b_{19} \\ b_{18} & b_{17} & b_{16} & b_{17} & b_{18} \\ b_{19} & b_{18} & b_{17} & b_{16} & b_{17} \\ b_{1,10} & b_{19} & b_{18} & b_{17} & b_{16} \end{vmatrix} .$$

Similar arguments show that the submatrices representative of the remaining array elements and element one, that is $\bar{\beta}_3, \bar{\beta}_4, \ldots, \bar{\beta}_{12}$, have the same form, symmetry and regularity as $\bar{\beta}_2$ and that there are only 5 distinct terms in each.

When the array is equally spaced, each of the remaining 48 submatrices in $\bar{\beta}$ is identical to one of the $\bar{\beta}_2, \bar{\beta}_3, \ldots \bar{\beta}_{12}$ submatrices discussed above. Thus, for an equally spaced array of straight parallel wires with equal segments, $\bar{\beta}$ consists of only 12 distinct submatrices, and in these, only 60 terms are distinct; it has the same Toeplitz property as its component submatrices.

$$\bar{\bar{\beta}} = \begin{vmatrix} \bar{\beta}_1 \bar{\beta}_2 \bar{\beta}_3 \bar{\beta}_4 \bar{\beta}_5 \bar{\beta}_6 \bar{\beta}_7 \bar{\beta}_8 \cdots \bar{\beta}_{12} \\ \bar{\beta}_2 \bar{\beta}_1 \bar{\beta}_2 \bar{\beta}_3 \bar{\beta}_4 \bar{\beta}_5 \bar{\beta}_6 \bar{\beta}_7 \cdots \bar{\beta}_{11} \\ \bar{\beta}_3 \bar{\beta}_2 \bar{\beta}_1 \bar{\beta}_2 \bar{\beta}_3 \bar{\beta}_4 \bar{\beta}_5 \bar{\beta}_6 \cdots \bar{\beta}_{10} \\ \cdots \\ \cdots \\ \cdots \\ \bar{\beta}_{12} \bar{\beta}_{11} \bar{\beta}_{10} \bar{\beta}_9 \bar{\beta}_8 \bar{\beta}_7 \bar{\beta}_6 \bar{\beta}_5 \cdots \bar{\beta}_1 \end{vmatrix} .$$

The cyclic property of $\bar{\bar{\beta}}$ and its submatrices is also present in the generalized impedance matrix $\bar{\bar{Z}}$ for this type of array (Strait and Hirasawa, 1969a), since elements in both $\bar{\bar{\beta}}$ and $\bar{\bar{Z}}$ depend only on intersegment distances.

The 60 distinct elements in $\bar{\bar{\beta}}$ are the first row b_{1m}, $1 \leq m \leq 60$, or the first column terms. These 60 terms are associated with four combinations of D_{nm} and E_{nm}:

(a) $D_{nm} = E_{nm} = 0$

(b) $D_{nm} \neq 0$, $E_{nm} = 0$

(c) $D_{nm} = 0$, $E_{nm} \neq 0$

(d) $D_{nm} \neq 0$, $E_{nm} \neq 0$.

These can be used to simplify the b_{nm} expression in Eq. (A4). Case (a) has been discussed earlier and constitutes the main diagonal terms in $\bar{\bar{\beta}}$ where $b_{nn} = 2/3$. Case (b) is the situation in 11 of the 60 required b_{nm} elements. They are $b_{1\alpha}$ where $\alpha = 6, 11, 16, \ldots, 56$.

Referring to the general b_{nm} expression in Eq. (A4), note that when $E_{nm} = 0$, all but the first ($i = 0$) term disappears and

$$b_{1\alpha} = \left(\frac{\pi}{2}\right)^{1/2} \left\{ \frac{J_{1/2}(D_{1\alpha})}{(D_{1\alpha})^{1/2}} - \frac{J_{3/2}(D_{1\alpha})}{(D_{1\alpha})^{3/2}} \right\},$$

for these 11 terms. But,

$$J_{1/2}(D_{1\alpha}) = \sqrt{\frac{2D_{1\alpha}}{\pi}} \frac{\sin D_{1\alpha}}{D_{1\alpha}}$$

and

$$J_{3/2}(D_{1\alpha}) = \sqrt{\frac{2D_{1\alpha}}{\pi}} \left\{ \frac{\sin D_{1\alpha}}{(D_{1\alpha})^2} - \frac{\cos D_{1\alpha}}{D_{1\alpha}} \right\}$$

Therefore,

$$b_{1\alpha} = \frac{1}{(D_{1\alpha})^2} \left\{ \frac{\sin D_{1\alpha}}{D_{1\alpha}} (D_{1\alpha}^2 - 1) + \cos D_{1\alpha} \right\} \tag{A5}$$

Note that Case (b), with $D_{nm} \neq 0$ and $E_{nm} = 0$ corresponds to elements of zero length, that is isotropic or short dipoles, and has been treated by Tai (1964) and Lo et al (1966). Equation (A5) agrees with their results. Case (c), $D_{nm} = 0$, $E_{nm} \neq 0$ arises in calculating 4 of the required 60 b_{nm} elements. They are $b_{1\beta}$, $\beta = 2, 3, 4, 5$. Looking at a general series representation for $J_\nu(x)$, that is,

$$J_\nu(x) = \sum_{r=0}^{\infty} \frac{(-1)^r x^{\nu+2r}}{r!\, 2^{\nu+2r}\, \Gamma(\nu+r+1)}$$

we see that

$$\frac{J_\nu(x)}{x^\nu} \to \frac{1}{2^\nu \Gamma(\nu+1)} \quad \text{as } x \to 0.$$

Hence, if in Eq. (A4) $D_{nm} = 0$, we have

$$b_{1\beta} = \sum_{i=0}^{\infty} \frac{(-1)^i (E_{1\beta})^{2i}}{(2i+1)!\ (i+3/2)}, \tag{A6}$$

where we have used the fact that

$$\frac{\pi^{1/2}}{2^{2i+1}\Gamma(i+1/2)\,\Gamma(i+1)} = \frac{1}{2\Gamma(2i+1)} .$$

The remaining 44 of the 60 required b_{nm} terms must be calculated from Eq. (A4). It is probably easier to simply use Eq. (A4) for all 60 b_{nm} terms when programming a computer for the calculations. In this case, fifteen terms of the series, Eq (A4), will provide sufficient accuracy, that is on the order of 10^{-8}, as long as the inter-element spacing is no smaller than $\lambda/3$. Calculations based on these results agreed with those based on the power gain formulation for the 12-element, lossless arrays considered in this paper.

Equations (A2) and (A4), together with the symmetry arguments and simplified b_{nm} forms, provide the basis for calculating the directive gain of an array of equally spaced straight wires with mutual coupling effects included. The final formula for this gain is given by:

$$G_D = \frac{V^+ (F\bar{Y})^+ (F\bar{Y})\,V}{V^+ (\bar{Y}^+ \bar{\beta}\,\bar{Y})\,V} \sin^2\theta .$$